Nonlinear tensor diffusion filter for the denoising of CT/MR images

S.N. Kumar*

Department of Electronics and Communication Engineering,
Sathyabama Institute of Science and Technology,
Chennai – 600119, Tamilnadu, India
Email: appu123kumar@gmail.com
*Corresponding author

A. Lenin Fred

School of Computer Science Engineering,
Mar Ephraem College of Engineering and Technology,
Elavuvilai – 629171, Marthandam, Tamilnadu, India
Email: lenifred.a@gmail.com

H. Ajay Kumar

School of Electronics and Communication Engineering,
Mar Ephraem College of Engineering and Technology,
Elavuvilai – 629171, Marthandam, Tamilnadu, India
Email: ajayhakkumar@gmail.com

P. Sebastin Varghese

Metro Scans and Laboratory,
Thiruvananthapuram, Kerala – 695011, India
Email: sebastin464@gmail.com

Abstract: The partial differential equation based algorithms play a prominent role in image processing and computer vision applications. The anisotropic diffusion technique was widely used for image enhancement and denoising. The Perona-Malika algorithm based on anisotropic diffusion fails to preserve sharp edges and fine details in the denoised image. In this paper, the variants of Perona-Malika (PM) model, nonlinear scalar diffusion (NLSD) filter and nonlinear tensor (NLTD) filter are analysed. The algorithms are analysed on sheep phantom image corrupted with Gaussian and Rician noise and results were validated by performance metrics like PSNR, MAE, EPI and MSSIM. The NLTD filter produces superior results when compared with NLSD and PM filter. The NLTD filter was also found to yield efficient restoration results for real-time CT/MR images and was validated by entropy measure.

Keywords: denoising; Perona-Malika; nonlinear scalar diffusion; NLSD; nonlinear tensor diffusion; NLTD; Rician noise; gauss gradient operator.

Reference to this paper should be made as follows: Kumar, S.N., Fred, A.L., Kumar, H.A. and Varghese, P.S. (2023) 'Nonlinear tensor diffusion filter for the denoising of CT/MR images', *Int. J. Advanced Intelligence Paradigms*, Vol. 24, Nos. 1/2, pp.156–172.

Biographical notes: S.N. Kumar is awarded his BE in Electrical and Electronics Engineering in 2007 and ME in Applied Electronics in 2011 from the Anna University, Chennai. He is a research scholar of Sathyabama Institute of Science and Technology, Chennai, Tamil Nadu, India in the Department of Electronics and Communication Engineering. His area of interest includes medical image processing and embedded system applications in telemedicine. He is working as an Assistant Professor in the Department of ECE at Mar Ephraem College of Engineering and Technology, Tamil Nadu, India and has seven years teaching experience. He is an active life member of BMESI, ISTE, ISRD, Bernoulli Society and IAENG. He is the Co-Principal Investigator of DST IDP funded project.

A. Lenin Fred received his BE in Computer Science and Engineering from the Madurai Kamaraj University in 1995, ME in Computer Science and Engineering from the Madurai Kamaraj University in 2001, Doctoral degree in Computer Science and Engineering, specialised in Digital Image Processing from the Manonmaniam Sundaranar University, Tirunelveli, India. His area of research includes medical image processing, biometrics and multimodal biometrics. He is working as Principal in Mar Ephraem College of Engineering Tamilnadu, India and he has 21 years of teaching experience. He is an active life member IEEE, ISTE, IET and ISRD. He is the Principal Investigator of several government funded projects.

H. Ajay Kumar is awarded his BE in Electronics and Communication Engineering in 2013 and ME in Applied Electronics in 2015 from the Anna University, Chennai. He is working as a Junior Research Fellow in the Department of ECE at Mar Ephraem College of Engineering and Technology, Tamil Nadu, India. His areas of interest are image processing and embedded system applications. He is an active life member of BMESI, ISTE, ISRD, and IAENG.

P. Sebastin Varghese is working as a Consultant Radiologist in Metro scans and Laboratories Pvt Ltd. His area of interest includes analysis of CT/MR image anomalies analysis and liver fat metabolism analysis.

This paper is a revised and expanded version of a paper entitled 'Denoising of abdomen CT/MR images using non linear tensor diffusion' presented at International Conference on Mathematical Modeling and Computational Methods in Science and Engineering, ICMMCMSE 2017, Alagappa University, Karaikudi, Tamilnadu, India, 20–22 February 2017.

1 Introduction

The role of partial differential equations (PDEs) is inevitable in computer vision and image processing especially in the domain of image restoration. The Gaussian filter is a linear diffusion approach in which the image is convolved with the Gaussian kernel. The concept of nonlinear diffusion evolves with the Perona-Malika restoration model; the object boundaries are preserved while smoothing the image (Bazan and Blomgre, 2008). A hybrid diffusion filter comprising of Perona-Malika diffusion and the bilateral filter was proposed for the denoising of images corrupted by Gaussian noise (Bazan and Blomgre, 2008).The denoising of MR images with intensity in homogeneity and artefacts was done by adaptive total variation-based filter and better results were produced (edges are also preserved) when compared to the Perona-Malika and total variation filter (Guo and Huang, 2009).The novel anisotropic diffusion model was proposed for 3D images based on the second derivative to determine the region boundary rather than gradient magnitude, efficient results were produced when compared with the gradient based techniques (Hossain and Möller, 2010).The modified diffusion model based on convection term was found to be efficient for the denoising of SEM and TEM images (Slavova and Rashkova, 2011).The variants of gradient denoising schemes; time delayed Perona-Malika model and nonlinear anisotropic tensor diffusion were analysed and efficient results were produced with edge preservation (Eymard et al., 2011).The fourth order PDE based anisotropic diffusion filter was proposed that minimises the staircase effect produced by the second order differential equation (Wang et al., 2012). The bilateral filter was found to be efficient for the Gaussian noise removal; however, it fails for the removal of speckle noise and salt and pepper noise (Bhonsle et al., 2012). The nonlinear filter that relies on homomorphic filter characteristics was found to be efficient for the denoising of Rican noise in MR images of the particular cartilage (Aarya et al., 2013). The selection of parameters is vital in anisotropic diffusion filter and various techniques were proposed for the selection of conductive coefficient, gradient threshold and a number of iterations (Tsiotsios and Petrou, 2013).The weighted anisotropic diffusion PDEs produces better restoration results with edge and texture features preservation (Prasath and Vorotnikov, 2014).A hybrid denoising scheme comprising of dual tree complex wavelet transform (DTCWT) and Wiener filter was proposed for the medical images (Naimi et al., 2015).The classical Perona-Malika algorithm was modified by a novel adaptive diffusion function for the denoising of medical images corrupted by Gaussian noise and Rician noise, and robust results were produced, when compared with the Perona-Malika, kernel anisotropic diffusion, non-local orientation diffusion, and double well potential algorithms (Heydari and Karami, 2015).The edge preservation is poor in the bilateral filter; however, the iterative bilateral filter is robust in the Rician noise removal of MR images (Riji et al., 2015). The nonlinear structure sensor based diffusion filter preserves the local features in the image restoration (Hahn and Lee, 2009).

This work proposes nonlinear tensor diffusion (NLTD) filter for the denoising of CT/MR images. Section 2 describes the Perona-Malika algorithm and its variants. Section 3 highlights the nonlinear scalar diffusion (NLSD) and NLTD filter algorithm characteristics and tuning of parameters. In Section 4, results and discussion are described; the algorithms are initially tested on Sheep Logan Phantom images corrupted by Gaussian and Rician noise of varying variance to determine the efficiency of the NLTD approach and then algorithms are also tested on real-time CT/MR images. Finally, conclusions are drawn in Section 5.

2 Related work

In image processing, a lot of spatial and transform domain filters are there for image restoration. Anisotropic filter based on partial differential equation proposed by Perona and Malika effectively reduces noise while preserving the edges (Perona and Malik, 1987, 1990). The 1D discrete representation of anisotropic filter derived from continuous diffusion process is as follows

$$\frac{\partial}{\partial t} I(x,t) = div[c(x,t) * gradI(x,t)] \tag{1}$$

$$\frac{\partial}{\partial t} I(x,t) = \phi_{\text{right}} - \phi_{\text{left}} \Big| \Delta x = 1 \tag{2}$$

The 2D diffusion filtering is simply the extension of 1D discrete implementation.

$$\frac{\partial}{\partial t} I(\bar{x},t) = div[c(\bar{x},t) * gradI(\bar{x},t)] \tag{3}$$

$$\frac{\partial}{\partial t} I(\bar{x},t) = \phi_{\text{east}} - \phi_{\text{west}} + \phi_{\text{north}} - \phi_{\text{south}} \tag{4}$$

The diffusion strength is regulated by $c(\bar{x},t)$ represents the spatial coordinates and t is the process ordering parameter.

The two commonly used diffusion coefficients are

$$C_1(x) = \exp\left\{-\left(\frac{x}{K}\right)^2\right\} \tag{5}$$

$$C_2(x) = \frac{1}{1+\left(\frac{x}{K}\right)^2} \tag{6}$$

The diffusion coefficient value depends on the image gradient magnitude and its value decreases with increase in gradient magnitude. The homogeneous regions of the images are smoothed with the same intensity in all directions. The diffusion coefficient $C_1(x)$ has better edge preserving capacity than $C_2(x)$. The parameter 'k' regulates the sensitivity to edges and its value is chosen based on the noise characteristics.

The 2D representation of anisotropic diffusion filter for the image $I(x, y)$ is as follows, the diffusion flow is determined only for the adjacent neighbours (four neighbourhood connectivity).

$$I_{x,y}^{t+1} = I_{x,y}^{t} + \lambda\left(\phi_N \nabla_{NI} + \phi_S \nabla_{SI} + \phi_E \nabla_{EI} + \phi_W \nabla_{WI}\right) \tag{7}$$

The better isotropy can be obtained when the diagonal neighbourhood pixels are also taken into account resulting in eight-way neighbourhood connectivity.

$$\begin{aligned} I_{x,y}^{t+1} = I_{x,y}^{t} + \lambda\big(&\phi_N \nabla_{NI} + \phi_S \nabla_{SI} + \phi_E \nabla_{EI} + \phi_W \nabla_{WI} \\ &+ \phi_{NE} \nabla_{NEI} + \phi_{SE} \nabla_{SEI} + +\phi_{SW} \nabla_{WSI} + +\phi_{NW} \nabla_{NWI}\big) \end{aligned} \tag{8}$$

The 2D diffusion filtering is efficient in the noise removal and edge preservation, but it creates staircase effect in the processed image. Perona-Malika equation is nonlinear and non-homogenous since the diffusion parameter $c(x, y, t)$ is a function of image data and time. In modified PM model, the input image was smoothed by the Gaussian filter before taking the gradient for better filtering results.

$$\nabla I_G = \nabla\left(G\sigma_g * I(x, y, t)\right) \tag{9}$$

where σ_g the standard deviation of Gaussian kernel and can be termed as regularisation parameter, which determines the uniform smoothing of the image.

The diffusion constant (Charbonnier et al., 1994; Blanc-Feraud et al., 1995) is expressed as follows

$$C(x, y, t) = \left(1 + \frac{|\nabla I_G|^2}{K^2}\right)^{-\frac{1}{2}} \tag{10}$$

The diffusion constant proposed by Weickert (1998) is as follows

$$C(x, y, t) = \begin{cases} 1 & ;\ \text{if} \left|\nabla I_G\right| = 0 \\ 1 - \exp\left(\dfrac{-C_\alpha}{\left(|\nabla I_G|^2 K^2\right)^m}\right) & ;\ \text{if} \left|\nabla I_G\right| > 0 \end{cases} \tag{11}$$

where the coefficient $C_\alpha > 0$, $\alpha = 4$ that implies $C_4 = 3.3148$ which gives visually good results.

The Turkeys' biweight conductance function (Black et al., 1998) as follows

$$C(x, y, t) = \begin{cases} \dfrac{1}{2}\left(1 - \left(\dfrac{\nabla I}{S}\right)^2\right)^2 & ;\ \nabla I \leq S \\ 10 & ;\ \text{otherwise} \end{cases} \tag{12}$$

where $S = \dfrac{K}{\sqrt{2}}$

The alpha Perona-Malika and adaptive Perona-Malika were proposed that can control the diffusion rate and can preserve the small features in the image (Tsiotsios et al., 2013; Guo et al., 2012).

3 Proposed methodology

The linear diffusion is a classical restoration model in which the image is convolved with the Gaussian kernel. The nonlinear diffusion model relies on the diffusion constant that is locally adapted and its effect becomes negligible as object boundaries are approached. The underlying principle of nonlinear diffusion is that diffusion stops as the object boundaries are reached. The PM is the classical nonlinear diffusion model and NLSD is the regularisation of PM model using Gaussian kernel termed as gauss gradient approach. The edge preservation is poor in the PM and NLSD models and hence tensor based nonlinear diffusion was proposed. The NLTD can be termed as an edge enhancing diffusion process that relies on the diffusion tensor for edge preservation. The diffusion tensor controls the rate of smoothing such that, across the edges, smoothing is minimised and along the edges smoothing is maximised. The NLTD algorithm produces superior results than the NLSD and the classical PM algorithm. The gauss gradient is the basic functionality for NLSD and NLTD algorithms.

3.1 Gauss gradient operation

In the gauss gradient, approach 1D kernel along *x* and *y*-direction are determined from the Gaussian function as follows

$$g(x, y) = \frac{1}{2\pi\sigma^2} e^{-\left(\frac{x_2 + y^2}{\sigma^2}\right)} \tag{13}$$

where σ represents the scale of diffusion

The Gaussian function in normalised form is as follows

$$g_s = e^{-(-x*x/2*\sigma^2)} \tag{14}$$

The first order derivative of the Gaussian function is as follows

$$I_x = \frac{\partial g_s}{\partial x} = \frac{-x}{\sigma^2} g_s \tag{15}$$

Similarly

$$I_y = \frac{\partial g_s}{\partial y} = \frac{-y}{\sigma^2} g_s \tag{16}$$

$$\frac{\partial^2 g_s}{\partial x} = \frac{x^2 - \sigma^2}{\sigma^4} g_s \tag{17}$$

The σ value is usually chosen greater than or equal to 1, can be scaled down to 0.7. The order of derivative is vital in the gauss gradient technique and up to second order derivatives are considered. The Gaussian smoothed image is obtained by the convolution with the generated kernel.

After Gaussian smoothing, the resultant image is represented as follows

$$I_G = \sqrt{Ix^2 + Iy^2} \tag{18}$$

where I_x and I_y are the Gaussian smoothed component of the image obtained from the convolution of the input image with the respective generated kernel along *x* and *y*-direction. The smoothed image by the gauss gradient operation is the basic building block of NLSD and NLTD restoration model.

3.2 Nonlinear scalar diffusion

The NLSD restoration model is represented as follows

$$\partial_t I = \nabla.(C\nabla I) \tag{19}$$

where *C* is the diffusion coefficient that depends on the gradient norm

$$C = \exp\left(-\frac{I_G}{K^2}\right) \tag{20}$$

The I_G is the Gaussian smoothed image and the edge preservation is influenced by proper selection of parameter K. The above partial differential equation in terms of the spatial component is represented as follows

$$\partial_t I = \partial_x \left(C \partial_x I\right) + \partial_y \left(C \partial_y I\right) \tag{20}$$

The NLSD restoration model in discrete form is expressed as follows

$$I_{i,j} = I_{i,j} + \frac{\lambda}{2}\left[C_1\left(I_{i+1,j}^t - I_{i,j}^t\right) - C_2\left(I_{i,j}^t - I_{i-1,j}^t\right) + C_3\left(I_{i,j+1}^t - I_{i,j}^t\right) - C_4\left(I_{i,j}^t - I_{i,j-1}^t\right)\right] \tag{21}$$

$$C_1 = \left(C_{i,j}^t - C_{i+1,j}^t\right) \tag{22}$$

$$C_2 = \left(C_{i-1,j}^t - C_{i,j}^t\right) \tag{23}$$

$$C_1 = \left(C_{i,j}^t - C_{i,j+1}^t\right) \tag{24}$$

$$C_1 = \left(C_{i,j-1}^t - C_{i,j}^t\right) \tag{25}$$

In the above expressions, the notation I_i, j represents the input image. The variable t represents the time and i, j are the spatial coordinates. Similarly, the diffusion coefficient is also represented in terms of time and spatial coordinates. The step size 'λ' plays a crucial role in the restoration result and is chosen lower than 0.25 to obtain a robust result.

3.3 Nonlinear tensor diffusion

The NLTD restoration model is represented as follows

$$\partial_t I = \nabla.(T \nabla I) \tag{26}$$

where T is a positive semi definite symmetric diffusion sensor. The pre-processing of 2D images are considered in this paper, hence T is a 2 × 2 matrix as follows

$$T = \begin{bmatrix} A & B \\ B & C \end{bmatrix} \tag{27}$$

where

$$A = \frac{c_1 G_x^2 + c_2 G_y^2}{I_G^2 + \varepsilon} \tag{28}$$

$$B = \frac{\left(c_2 - c_1\right) G_x G_y}{I_G^2 + \varepsilon} \tag{29}$$

$$C = \frac{c_1 G_y^2 + c_2 G_x^2}{I_G^2 + \varepsilon} \tag{30}$$

The term I_G represents the Gaussian smoothed version of the input image and G_x, G_y are the components of I_G. The terms c_1 and c_2 are the diffusion constants.

$$c_1 = \exp\left(-\left(\frac{I_G}{K}\right)^2\right) \tag{31}$$

$$c_2 = \frac{1}{5} * c_1 \tag{32}$$

The element of tensors are functions of the image characteristics. The NLTD in terms of Cartesian coordinates are as follows

$$\partial_t I = \begin{bmatrix} \partial_x & \partial_y \end{bmatrix} \begin{bmatrix} A & B \\ B & C \end{bmatrix} \begin{bmatrix} \partial_x I \\ \partial_y I \end{bmatrix} \tag{33}$$

$$\partial_t I = \begin{bmatrix} \partial_x & \partial_y \end{bmatrix} \begin{bmatrix} A\partial_x I & B\partial_y I \\ B\partial_x I & C\partial_y I \end{bmatrix} \tag{34}$$

$$\partial_t I = \partial_x \left(A\partial_x I + B\partial_y I\right) + \partial_y \left(B\partial_x I + C\partial_y I\right) \tag{35}$$

$$\partial_t I = \partial_x \left(A\partial_x I\right) + \partial_x \left(B\partial_y I\right) + \partial_y \left(B\partial_x I\right) + \partial_y \left(B\partial_y I\right) \tag{36}$$

while comparing this partial differential equation with the NLSD model, two new terms arise $\partial_x(\mathrm{B}\partial_y I)$ and $\partial_y(\mathrm{B}\partial_x I)$.

The NLTD restoration model in discrete form is as follows

$$\begin{aligned} I_{i,j}^{t+\lambda} = I_{i,j}^{t} + \lambda\big[& B_1 I_{i-1,j+1} + C_1 I_{i,j+1} + B_2 I_{i+1,j+1} + A_1 I_{i-1,j} \\ & -\left(\frac{A_{i-1,j} + 2A_{i,j} + A_{i+1,j} + C_{i-1,j} + 2C_{i,j} + C_{i+1,j}}{2}\right) \\ & I_{i,j} + A_2 I_{i+1,j} + B_3 I_{i-1,j-1}\big] \end{aligned} \tag{37}$$

where

$$A_1 = \frac{A_{i-1,j} + B_{i,j}}{4} \tag{38}$$

$$A_2 = \frac{A_{i+1,j} + A_{i,j}}{2} \tag{39}$$

$$B_1 = \frac{-B_{i-1,j} + B_{i,j+1}}{4} \tag{40}$$

$$B_2 = \frac{B_{i+1,j} + B_{i,j+1}}{4} \tag{41}$$

$$B_3 = \frac{B_{i-1,j} + B_{i,j+1}}{4} \tag{42}$$

$$C_1 = \frac{C_{i,j+1} + C_{i,j}}{2} \tag{43}$$

From the expression, it is clear that all the terms in the right hand side of the equation are linear for the values of $I_{i,j}$. The discrete form of the NLTD restoration model is represented in terms of a quasi-convolution kernel since the values in the 3 × 3 kernel are dependent on the elements of the tensor matrix and spatial positions.

4 Result and discussion

The pre-processing algorithms are tested on the Sheep Logan phantom images corrupted with Gaussian and Rician noise and on real-time abdomen CT/MR medical images. From the Sheep Logan phantom image, the noisy input image was generated by adding Gaussian noise with the standard deviation (σ_g) and Rician noise with the standard deviation (σ_R) for the validation of restoration algorithms. The algorithms are developed in MATLAB R20101a software running on the Windows PC with core i3 processor, 4 GB RAM specification.

The median, bilateral and Gaussian filters are widely used for the removal of noise in medical images, however, blur occurs in boundaries and edge preservation is also poor. In Hu et al. (2012), it was reported that PM restoration model outperforms median filter (kernel size 5 × 5), Wiener filter (kernel size 5 × 5) and Gaussian filter for sheep Logan phantom images corrupted by Gaussian noise in terms of Root Mean Square Error (RMSE). The results below depicts the efficiency of NLTD filter in terms of PSNR, MSE and MAE when compared with the PM and NLSD filtering approaches. The algorithms have been tested on real-time CT/MR DICOM images. The images are obtained from the Metro Scans and Research Laboratory, Thiruvananthapuram. The CT images of the abdomen are obtained from Optima CT machine with a slice thickness of 0.6 mm. The two data sets of the abdomen are used in this work and each dataset comprises of 200 images. The results of typical slices are depicted here. The MR images of knee are obtained from GE healthcare 1.5T machine with a slice thickness of 1.2 mm. The two data sets of knee are used in this work and the results of typical slices are depicted here.

The expression for PSNR and MAE are expressed as follows.

$$PSNR = 10\log\left(\frac{255^2 y_0 y_1}{\|y_0 - y_1\|^2}\right)dB \tag{44}$$

$$MAE = \frac{\|y_0 - y_1\|}{XY} \tag{45}$$

where y_0 and y_1 are the input phantom image and the denoised image. Higher value of PSNR and lower value of MSE, MAE indicates the efficient of denoising algorithm. The tuning of parameters for restoration algorithms are depicted in Table 1.

Table 1 Restoration algorithms and tuning of parameters

Algorithm		*Parameters*
Perona-Malika filter	1	Number of iterations: 15
	2	Kappa(Gradient Modulus threshold that controls the conduction value): 20 ≤ Kappa ≤ 100, Kappa = 30
	3	Step size(λ: integration constant): 0 ≤ λ ≤ 1/7, λ = 0.24
	4	Conduction coefficient: two choices $C_1(x)$ and $C_2(x)$, $C_1(x)$ is used which has better edge preservation capacity
Nonlinear scalar diffusion filter	1	Number of iterations: 15
	2	Edge strength (K): K > 0, larger value of K leads to isotropic solution, K = 0.1
	3	λ (Integration Constant): 0 ≤ λ ≤ 1/7, λ = 0.24
Nonlinear tensor diffusion filter	1	Number of iterations: 15
	2	Edge strength (K): K > 0, larger value of K leads to isotropic solution, K = 0.1
	3	λ (Integration Constant): 0 ≤ λ ≤ 1/7, λ = 0.24
	4	Uscale (standard deviation of Gaussian function): 0.7 ≤ Uscale ≤ 1.4, Uscale = 1.2

The increase in number of iterations will create a blurring effect in the restored image and in this work, 15 iterations are chosen. The higher value of kappa also induces blurring effect in the restored image and hence an optimum value of 30 is used in this work. The step size (λ) indicates the stability of solution and normally λ = 0.24 to 0.25 is used in many cases. The higher value of K will preserve the wider edges only and fine edges are neglected. Hence, here in this work, an optimum value of K = 0.1 is used. Table 2 depicts the PSNR, MSE and MAE determined between the input and noisy phantom images. The performance metrics are determined for the Gaussian and Rician noise distribution with the noise variance ranging from 0.01 to 0.20. The performance metrics for Sheep Logan Phantom image are depicted in Table 2.

Table 2 Performance metrics calculated between Sheep Logan phantom input and its noisy version

Noise type	*Metrics*	*Noise variance*					
		0.01	*0.04*	*0.08*	*0.12*	*0.16*	*0.20*
Gaussian noise	PSNR	21.1926	20.0229	18.1144	16.2477	14.6176	13.1564
	MSE	0.0076	0.0099	0.0154	0.0237	0.0345	0.0483
	MAE	0.0600	0.0719	0.0960	0.1258	0.1594	0.1955
Rician noise	PSNR	35.1167	25.7217	19.9201	16.4920	14.0266	12.0787
	MSE	0.0003	0.0027	0.0102	0.0224	0.0396	0.0620
	MAE	0.0117	0.0431	0.0850	0.1259	0.1667	0.2082

The PSNR comparisons for variants of PM models are represented in Table 3. From the table, it is evident that NLTD filter has high PSNR when compared with the PM and NLSD filter. Here the PSNR is determined between the input and the denoised input image.

Table 3 PSNR values for Perona-Malika, NLSD and NLTD restoration models

Noise type	*Metrics*	*Noise variance*					
		0.01	*0.04*	*0.08*	*0.12*	*0.16*	*0.20*
Gaussian noise	PM	21.0960	20.3035	18.6563	18.7191	15.1556	13.592
	NLSD	24.8540	23.1540	20.2951	20.4033	15.6721	13.8665
	NLTD	26.0313	23.8605	20.6441	20.7288	15.7908	13.9454
Rician noise	PM	21.7043	20.1262	18.5328	16.9644	16.1002	15.3119
	NLSD	23.8239	22.7096	19.8702	17.6478	16.5314	15.5527
	NLTD	24.9145	23.9089	20.4391	17.9522	16.7341	15.6960

By comparing the PSNR values in Table 3 with the PSNR values in Table 2, there is an improvement in the PSNR value, which shows the proficiency of NLTD filter. The MSE values of the filtering algorithms in Table 4 also indicates the efficiency of the NLTD algorithm. The MSE values significantly decrease when compared with the MSE values in Table 2.

Table 4 MSE values for Perona-Malika, NLSD and NLTD restoration models

Noise type	*Metrics*	*Noise Variance*					
		0.01	*0.04*	*0.08*	*0.12*	*0.16*	*0.20*
Gaussian noise	PM	0.0078	0.0093	0.0136	0.0134	0.0305	0.0437
	NLSD	0.0033	0.0048	0.0093	0.0091	0.0271	0.0411
	NLTD	0.0025	0.0041	0.0086	0.0085	0.0264	0.0403
Rician noise	PM	0.0068	0.0097	0.0140	0.0201	0.0245	0.0294
	NLSD	0.0021	0.0054	0.0103	0.0172	0.0222	0.0278
	NLTD	0.0010	0.0041	0.0090	0.0160	0.0212	0.0269

Similarly, the MAE values also indicates that NLTD filter performs better for the filtering of Gaussian noise in CT images and Rician noise in MR images. The values of MAE for NLTD algorithm are low when compared with the values of MAE in Table 2.

Table 5 MAE values for Perona-Malika, NLSD and NLTD restoration models

Noise type	*Metrics*	*Noise variance*					
		0.01	*0.04*	*0.08*	*0.12*	*0.16*	*0.20*
Gaussian noise	PM	0.0620	0.0750	0.1001	0.0990	0.1627	0.1981
	NLSD	0.0450	0.0596	0.0888	0.0874	0.1583	0.1963
	NLTD	0.0415	0.0566	0.0867	0.0854	0.1565	0.1947
Rician noise	PM	0.0471	0.0706	0.0949	0.1179	0.1347	0.1507
	NLSD	0.0276	0.0583	0.0875	0.1144	0.1333	0.1511
	NLTD	0.0218	0.0532	0.0834	0.1113	0.1307	0.1489

The edge preservation of restoration algorithms was validated by edge preservation index (EPI) (Zhu and Rao, 2015).The EPI indicates the edge preservation after the noise reduction by applying a restoration algorithm. For perfect edge preservation, EPI value will be '1'. Table 6 depicts that, NLTD restoration algorithm is having a higher value of EPI when compared with the PM and NLSD algorithms.

$$EPI = \frac{\sum\left(\Delta y_0 - \Delta\overline{y_0}\right)\left(\Delta y_1 - \Delta\overline{y_1}\right)}{\sqrt{\sum\left(\Delta y_0 - \Delta\overline{y_0}\right)^2 \sum\Delta\left(\Delta y_1 - \Delta\overline{y_1}\right)^2}}$$

where y_0 is the original image, $\overline{y_0}$ represents the mean of y_0, y_1 is the original image, $\overline{y_1}$ represents the mean of y_1.

The EPI values for restoration algorithms are depicted in Table 6.

Table 6 EPI values for Perona-Malika, NLSD and NLTD restoration models

Noise type	*Metrics*	*Noise variance*					
		0.01	*0.04*	*0.08*	*0.12*	*0.16*	*0.20*
Gaussian noise	PM	0.1112	0.1014	0.0935	0.0935	0.0835	0.0786
	NLSD	0.8556	0.8576	0.8490	0.8328	0.8122	0.7922
	NLTD	0.8655	0.8667	0.8566	0.8408	0.8225	0.8017
Rician noise	PM	0.4062	0.2449	0.1448	0.0952	0.0753	0.0563
	NLSD	0.9494	0.9329	0.8755	0.7879	0.6931	0.5936
	NLTD	0.9612	0.9379	0.8873	0.8221	0.7487	0.6805

The multi-scale structural similarity index (MSSIM) represents the similarity between the input and the denoised image (Wang et al., 2003). The MSSIM was proposed by Wang and Bovik and it incorporates SSIM evaluations at different scale. The higher the value of MSSIM (closer to '1') indicates the efficiency of restoration algorithm.

Table 7 MSSIM values for Perona-Malika, NLSD and NLTD restoration models

Noise type	*Metrics*	*Noise variance*					
		0.01	*0.04*	*0.08*	*0.12*	*0.16*	*0.20*
Gaussian noise	PM	0.964	0.968	0.967	0.961	0.967	0.962
	NLSD	0.975	0.972	0.971	0.980	0.977	0.986
	NLTD	0.997	0.994	0.992	0.998	0.991	0.993
Rician noise	PM	0.959	0.958	0.954	0.964	0.968	0.967
	NLSD	0.969	0.964	0.975	0.971	0.987	0.985
	NLTD	0.995	0.997	0.991	0.989	0.992	0.993

The MSSIM index is expressed as follows.

$$\text{MSSIM} = \prod_{i=1}^{M} (\text{SSIM}_i)^{\beta_i}$$

where the value of β_i are estimated through psychophysical measurement.

$$\text{SSIM}_i = \begin{cases} \frac{1}{N_i}\sum C\left(p_{i,j}, q_{i,j}\right) S\left(p_{i,j}, q_{i,j}\right); i = 1, 2, 3 \dots . M - 1 \\ \frac{1}{N_i}\sum L\left(p_{i,j}, q_{i,j}\right) C\left(p_{i,j}, q_{i,j}\right) CS\left(p_{i,j}, q_{i,j}\right); i = M \end{cases}$$

The $p_{i,j}$ and $q_{i,j}$ represents j^{th} local image patches at the i^{th} scale, N_i be the number of evaluation windows in the scale.

The $L(p_{i,j}, q_{i,j})C(p_{i,j}, q_{i,j})$ and $S(p_{i,j}, q_{i,j})$ represents the luminance contrast and structural similarities.

The restoration algorithms output for Sheep Logan Phantom image corrupted by Gaussian noise is depicted in Figure 1.

Figure 1 (a) Gaussian noise added Sheep Logan phantom image and its colour map (b) PM output and its colour map (c) NLSD output and its colour map (d) NTLD output and its colour map (see online version for colours)

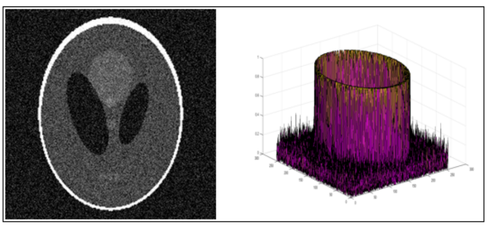

(a)

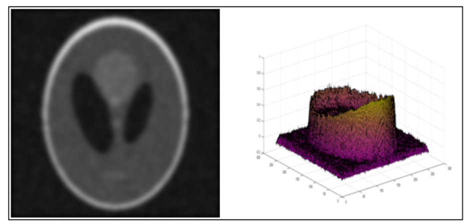

(b)

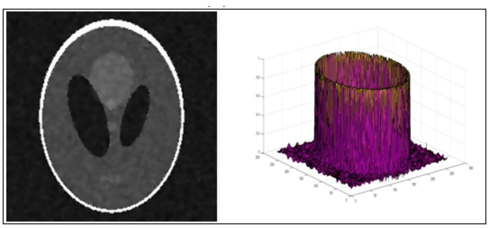

(c)

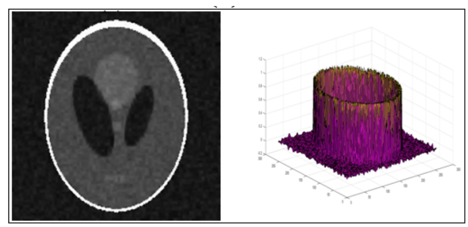

(d)

Figure 2 (a) Rician noise added Sheep Logan phantom image and its colour map (b) PM output and its colour map (c) NLSD output and its colour map (d) NTLD output and its colour map (see online version for colours)

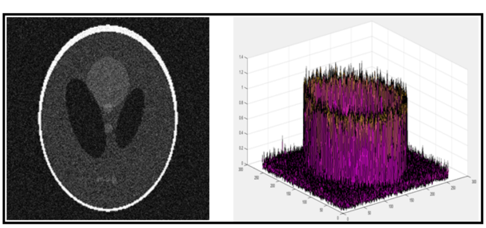

(a)

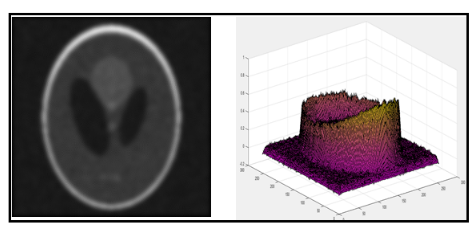

(b)

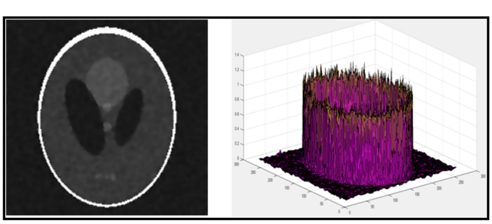

(c)

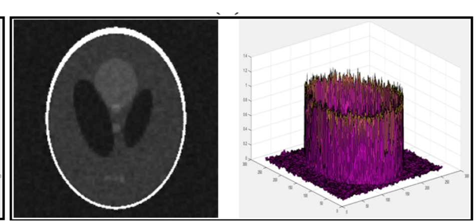

(d)

The restoration algorithms output for Sheep Logan Phantom image corrupted by Rician noise is depicted in Figure 2.

The ID1, ID2 represents the real-timeCT liver datasets and ID3, ID4 represents the real-timeMR knee datasets. The NLTD restoration algorithm output for real-time CT/MR images are depicted in Figure 3.

The performance of the filtering of real-time medical images was validated by entropy measure. Lower the entropy, better is the restoration algorithm. The NLTD filter was found to have lower entropy when compared with the PM and NLSD model.

Figure 3 (a) Input CT image and its colour map (b) NTLD output and its colour map (c) Input MR image and its colour map (d) NTLD output and its colour map (see online version for colours)

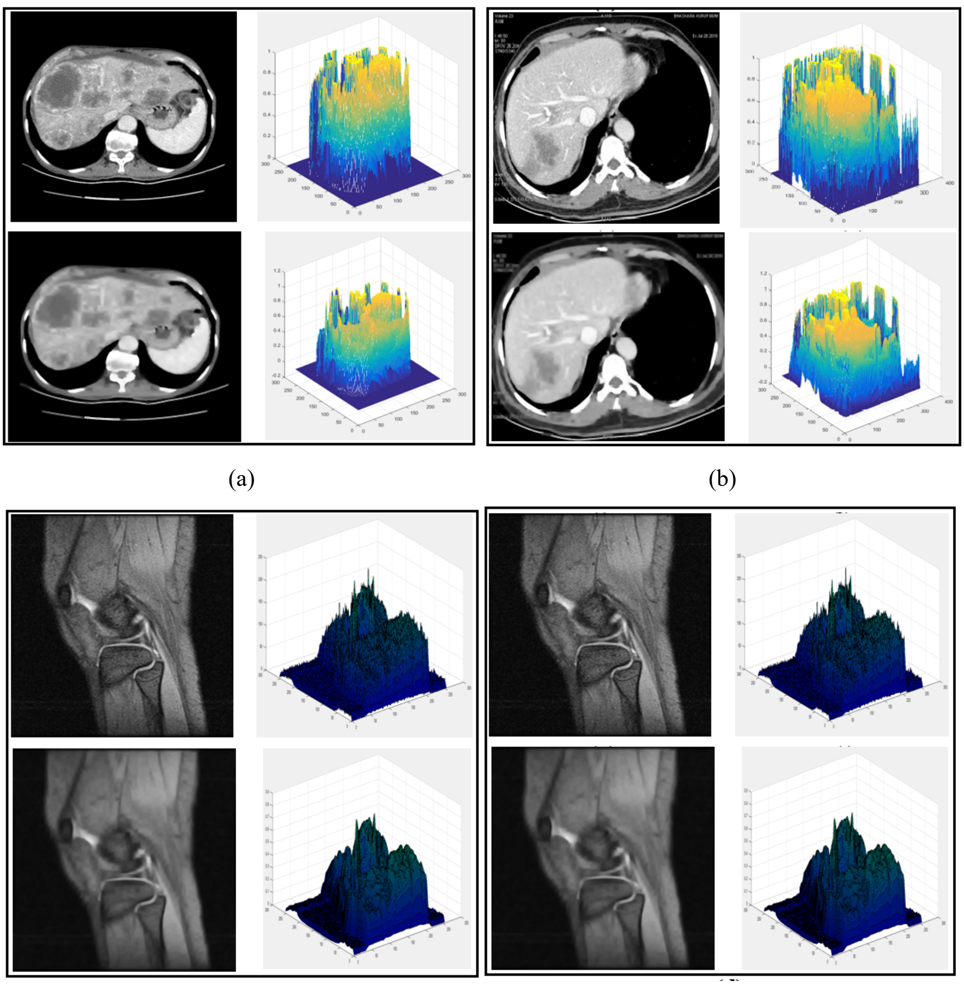

(a) (b)

(c) (d)

Figure 4 (a) Input CT image and its colour map (b) NLSD output and its colour map (c) Input MR image and its colour map (d) NLSD output and its colour map (see online version for colours)

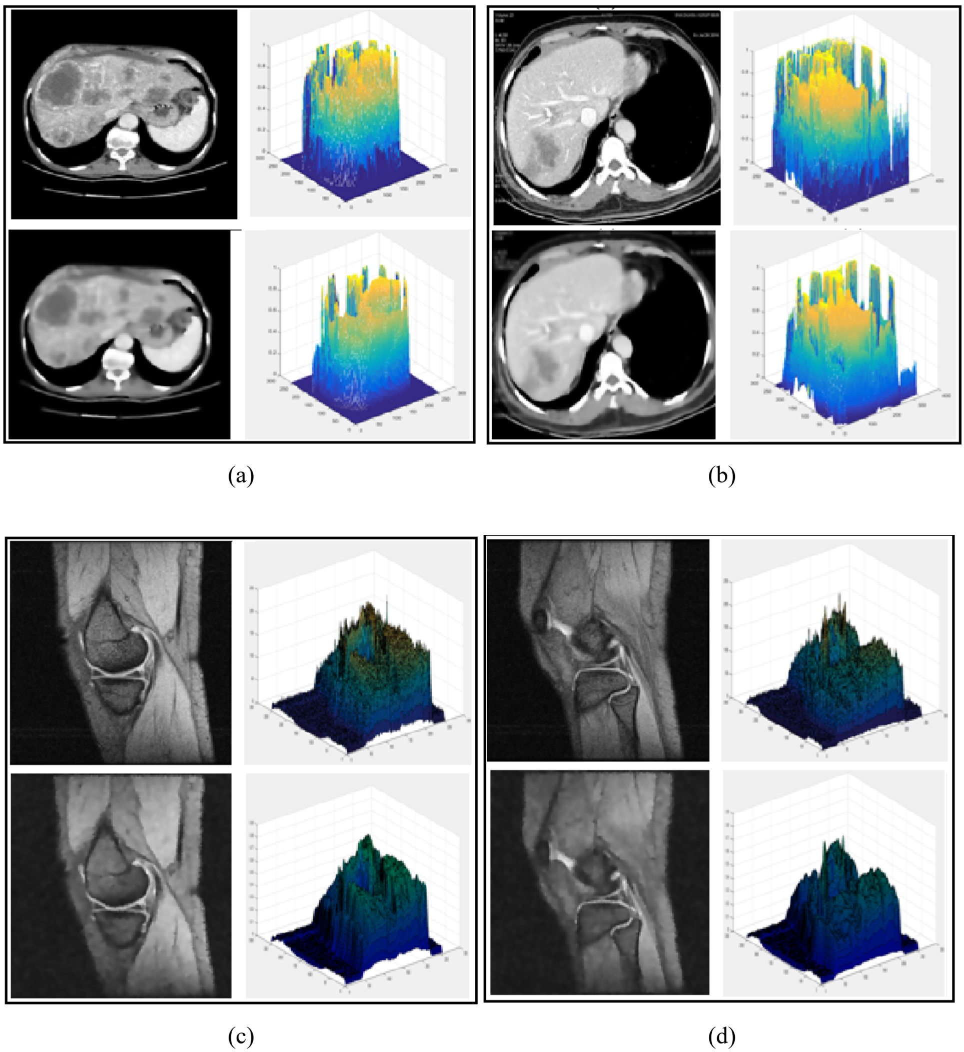

Table 8 Entropy values for Perona-Malika, NLSD and NLTD restoration models

Dataset ID	*Input*	*Perona-Malika*	*NLSD*	*NLTD*
ID1	4.3859	4.7301	4.8233	4.4392
ID2	5.9926	7.2936	6.6418	6.2525
ID3	6.8251	6.4098	6.3704	6.3437
ID4	7.0464	6.6897	6.6097	6.5620

5 Conclusions

This paper proposes variants of PM restoration model for the denoising of CT/MR images. The role of denoising is vital for image processing applications like segmentation and compression. The performance of the algorithms was evaluated by performance metrics like PSNR, MSE, MAE, EPI and MSSIM. The NLTD restoration model was found to have high PSNR, high EPI, high MSSIM, low MSE and low MAE for Sheep Logan Phantom images corrupted by Gaussian and Rician noise. The NLTD restoration model produces satisfactory results for the denoising of real-time CT/MR images with good edge preservation. The lower value of entropy reveals the efficiency of NLTD filter for the real-time CT/MR images. The future work will be the hardware implementation of NLTD filter for telemedicine applications.

Acknowledgements

The authors would like to acknowledge the support provided by DST under IDP scheme (No: IDP/MED/03/2015). We thank Dr Sebastian Varghese (Consultant Radiologist, Metro Scans and Laboratory, Trivandrum) for providing the medical CT images and supporting us in the preparation of manuscript.

References

Aarya, I., Jiang, D. and Gale, T. (2013) 'Signal dependent Rician noise denoising using nonlinear filter', *Lecture Notes on Software Engineering*, Vol. 1, No. 4, pp.344–349.

Bazan, C. and Blomgre, P. (2008) *Image Smoothing and Edge Detection by Nonlinear Diffusion and Bilateral Filter*, ACSESS.

Bhonsle, D., Chandra, V. and Sinha, G.R. (2012) 'Medical image denoising using bilateral filter', *I.J. Image, Graphics and Signal Processing*, Vol. 4, No. 6, pp.36–43.

Black, M.J., Sapiro, G., Marimont, D. and Heeger, D. (1998) 'Robust anisotropic diffusion', *IEEE Transactions on Image Processing*, Vol. 7, No. 3, pp.421–432.

Blanc-Feraud, L., Charbonnier, P., Aubert, G. and Barlaud, M. (1995) 'Nonlinear image processing: modeling and fast algorithm for regularization with edge detection', *Proceedings International Conference on Image Processing*, pp.23–26.

Charbonnier, P., Blanc-Feraud, L., Aubert, G. and Barlaud, M. (1994) 'Two deterministic half-quadratic regularization algorithms for computed imaging', *Proceedings IEEE International Conference on Image Processing*, ICIP-94, pp.13–16.

Eymard, R., Handlovicova, A., Herbin, R., Mikula, K. and Stasova, O. (2011) 'Gradient schemes for image processing', in Fořt, J., Fürst, J., Halama, J., Herbin, R. and Hubert, F. (Eds.): *Finite Volumes for Complex Applications VI Problems & Perspectives*, *Springer Proceedings in Mathematics*, Vol. 4, pp.429–437, Springer, Berlin, Heidelberg.

Guo, W. and Huang, F. (2009) 'Adaptive total variation based filtering for MRI images with spatially, inhomogeneous noise and artifacts', *IEEE International Symposium on Biomedical Imaging: from Nano to Macro*.

Guo, Z., Sun, J., Zhang, D. and Wu, B. (2012) 'Adaptive Perona-Malik model based on the variable exponent for image denoising', *IEEE Transactions on Image Processing*, Vol. 21, No. 3, pp.958–967.

Hahn, J. and Lee, C.O. (2009) 'A nonlinear structure tensor with the diffusivity matrix composed of the image gradient', *Journal of Mathematical Imaging and Vision*, Vol. 34, No. 2, pp.137–51.

Heydari, M. and Karami, M.R. (2015) 'A new adaptive diffusive function for magnetic resonance imaging denoising based on pixel similarity', *Journal of Medical Signals and Sensors*, Vol. 5, No. 4, pp.201–209.

Hossain, Z. and Möller, T. (2010) 'Edge aware anisotropic diffusion for 3D scalar data', *IEEE Transactions on Visualization and Computer Graphics (Proceedings Visualization/ Information Visualization 2010)*, Vol. 16, No. 6, pp.1375–1384.

Hu, S., Liao, Z. and Chen, W. (2012) 'Sinogram restoration for low-dosed X-ray computed tomography using fractional-order Perona-Malik diffusion', *Hindawi Publishing Corporation Mathematical Problems in Engineering*.

Naimi, H., Adamou-Mitiche, A.B.H. and Mitiche, L. (2015) 'Medical image denoising using dual tree complex thresholding wavelet transform and Wiener filter', *Journal of King Saud University – Computer and Information Sciences*, Vol. 27, No. 1, pp.40–45.

Perona, P. and Malik, J. (1987) 'Scale-space and edge detection using anisotropic diffusion', in *Proceedings, IEEE Computer Society workshop on Computer Vision*, pp.16–27.

Perona, P. and Malik, J. (1990) 'Scale-space and edge detection using anisotropic diffusion', *IEEE Transactions on Pattern Analysis and Machine Intelligence*, Vol. 12, No. 7, pp.629–639.

Prasath, V.B.S. and Vorotnikov, D. (2014) 'Weighted and well-balanced anisotropic diffusion scheme for image denoising and restoration', *Nonlinear Analysis: Real World Applications*, Vol. 17, No. 1, pp.33–46.

Riji, R., Rajan, J., Sijbers, J. and Nair, M.S. (2015) 'Iterative bilateral filter for Rician noise reduction in MR images', *Signal, Image and Video Processing*, October, Vol. 9, No. 7, pp.1543–1548.

Slavova, A. and Rashkova, V. (2011) 'A novel PDE-based image denoising model with applications in nanoindustry', *Mathematica Balkanica*, Vol. 25, No. 3, pp.317–328.

Tsiotsios, C. and Petrou, M. (2013) 'On the choice of the parameters for anisotropic diffusion in image processing', *Pattern Recognition*, Vol. 46, No. 5, pp.1369–1381.

Wang, H., Wang, Y. and Ren, W. (2012) 'Image denoising using anisotropic second and fourth order diffusions based on gradient vector convolution', *ComSIS*, Vol. 9, No. 4, Special Issue, pp.1493–1511.

Wang, Z., Simoncelli, E.P. and Bovik, A.C. (2003) 'Multi-scale structural similarity for image quality assessment', *Inasilomar Conference on Signals Systems and Computers*, IEEE, 9 November, Vol. 2, pp.1398–1402.

Weickert, J. (1998) *Anisotropic Diffusion in Image Processing*, B.G. Teubner Stuttgart, Leipzig, Germany.

Zhu, H.J. and Rao, L. (2015) 'Ultrasonic liver image denoising based on a hybrid threshold method', *International Conference on Power Electronics and Energy Engineering*, Atlantis Press, pp.139–142.